Nanoscale

This is an *Accepted Manuscript*, which has been through the Royal Society of Chemistry peer review process and has been accepted for publication.

Accepted Manuscripts are published online shortly after acceptance, before technical editing, formatting and proof reading. Using this free service, authors can make their results available to the community, in citable form, before we publish the edited article. We will replace this *Accepted Manuscript* with the edited and formatted *Advance Article* as soon as it is available.

You can find more information about *Accepted Manuscripts* in the **Information for Authors**.

ARTICLE TYPE

Molecular hot electroluminescence due to strongly enhanced spontaneous emission rates in a plasmonic nanocavity

Gong Chen,[a] **Xiaoguang Li,**[a,b] **Zhenyu Zhang,**[a] **and Zhenchao Dong** [*a]

Revised 16th December 2014

We demonstrated recently anomalous relaxationless hot electroluminescence from molecules in the tunnel junction of a scanning tunneling microscope [Dong *et al., Nature Photonics*, 2010, **4**, 50]. In the present paper, based on physically realistic parameters, we aim to unravel the underlying physical mechanism by using a multiscale modeling approach that combines classical generalized Mie theory with quantum master equation. We find that the nanocavity-plasmon-tuned spontaneous emission rate plays a crucial role in shaping the spectral profile. In particular, on resonance, the radiative decay rate can be enhanced by three-to-five orders of magnitude, which enables the radiative process to occur on the lifetime scale of picoseconds and become competitive to the vibrational relaxation. Such a large Purcell effect opens up new emission channels to generate the hot luminescence that arises directly from higher vibronic levels of the molecular excited state. We also stress that the critical role of resonant plasmonic nanocavities in tunneling electron induced molecular luminescence is to enhance the spontaneous radiative decay through plasmon enhanced vacuum fluctuations rather than to generate an efficient plasmon stimulated emission process. This improved understanding has been partly overlooked in previous studies but is believed to be very important for further developments of molecular plasmonics and optoelectronics.

1 Introduction

For over two decades, much attention has been drawn on the light emission from the tunnel junction of a scanning tunneling microscope (STM) thanks to its potential to provide insights into the nature of transport and photonics at the nanoscale. Ever since the first experimental evidence of the STM induced luminescence (STML),[1] extensive research has been carried out on the electroluminescence (EL) on metal surfaces,[2,3] nanoparticles,[4] metallic quantum wells,[5] etc. It is well accepted that the light emission in the tunneling junction arises from the radiative decay of the localized surface plasmon (LSP), via the excitation of inelastic tunneling electrons.[6–9] As the LSP resonance is known to depend on the size, shape and dielectric properties of metallic nanostructures, we can thus tune the light emission characteristics by controlling the geometry of the nanocavity defined by the tip and substrate.[10]

On the other hand, the pursuit of nanoscale molecular optoelectronics has stimulated a lot of interests in applying the STML technique to the study of molecular luminescence from the nanocavity defined by the STM tunnel junction.[11–15] If both the lowest unoccupied molecular orbital (LUMO) and highest occupied molecular orbital (HOMO) lie inside the bias voltage window of the junction, the molecule can be effectively excited by the simultaneous tunneling of one electron into LUMO and the other out of HOMO.[13] The light emission property from the molecular junction is also found to depend not only on the intrinsic electronic structure of the molecule, but also on its local nanocavity environment.[16–18] Recently, we have further demonstrated that such profound modulation of molecular emission profiles by resonant nanocavity plasmons can even generate the relaxationless hot luminescence (HL) from highly excited vibrational levels (i.e., the luminescence from non-thermalized excitons).[19] This observation is against the Kasha's rule in conventional molecular fluorescence and has raised demands for understanding its mechanism related to ultrafast emission processes. In a first treatment, a model based on the rate-equation formalism was proposed, ignoring the effect of plasmons.[20] The authors stated that the HL phenonmenon can occur as soon as the vibrational relaxation rate becomes comparable to the electron transmission rate at around 10^{10} s^{-1}. Subsequent treatments took into account the role of plasmons.[21–23] Zhang *et al.*[23] explained plasmon enhanced electroluminescence by using a configuration with a single molecule contacted to two electrodes and also sandwiched between two metal nanoparticles. On the other hand, Tian *et al.*[21,22] adopted a more realistic model used in the STML experiment and attributed the hot luminescence to the stimulated emission of molecules by the plasmonic field, in which the plasmon also acts as an additional excitation source other than tunneling electrons. However, since the gap distance becomes considerably larger upon the

---

[a] *International Center for Quantum Design of Functional Materials, Hefei National Laboratory for Physical Sciences at the Microscale, University of Science and Technology of China, Hefei, Anhui, 230026, China. E-mail: zcdong@ustc.edu.cn*
[b] *Shenzhen Institutes of Advanced Technology, Chinese Academy of Sciences, Shenzhen, 518055, China.*

insertion of a decoupled molecule, the plasmonic field excited directly by inelastic tunneling electrons is probably very weak and it is still an open issue to what extent the plasmon can come back to excite the molecule. The generation of HL is even more challenging, and therefore, the mechanism for the HL still remains to be further explored.

In this paper, we provide a physically more plausible mechanism for the hot electroluminescence we observed recently, which stresses on the spontaneous emission of the excited molecule in a plasmonic nanocavity but without involving the molecular excitation by plasmons. We investigate the light emission of a molecule (i.e., a two-level quantum emitter) induced by tunneling currents from a nanocavity defined by the junction of two metal nanospheres. Our calculations are based on a multiscale modeling approach that combines classical electrodynamics with quantum mechanics, using physically realistic parameters. By adopting electromagnetic simulations based on generalized Mie theory,[24] we show that in the tunneling junction, the spontaneous decay rate of the molecule can be strongly enhanced by tuning the geometry and material of the nanocavity. Furthermore, within the framework of the quantum master equation,[25] we consider both the spontaneous emission and vibrational damping processes of a model molecule with two electronic levels and one vibrational mode. We find that, in contrast to Kasha's rule, the excited molecule can directly decay radiatively to the ground state without vibrational relaxation due to the largely enhanced spontaneous emission rate in some special nanocavities, leading to the occurrence of hot luminescence.[19] In particular, we stress that this effect is due to the enhancement in plasmonic vacuum field rather than plasmon stimulated emission. Such improved understanding not only provides a possible explanation for the observed HL phenomenon, but may also be instructive for further studies in STML as well as single-molecule optoelectronics and photonics.

This paper is organized as follows. In Sec. 2, we introduce theoretical methods that include the generalized Mie theory and the quantum master equation, taking into account electron tunneling and various damping processes. In Sec. 3, we discuss the relation between the spontaneous decay rate and the nanocavity plasmon in the STM junction. The influence of resonant nanocavity plasmons on both the spectral profile of molecular electroluminescence and the generation of molecular HL is presented and discussed in detail in Sec. 4, which is followed by concluding remarks in Sec. 5.

2 Theoretical model

The HL was experimentally observed in a system with a multilayer of molecules between the STM tip and metal substrate, with the bottom layers of molecules acting as a spacer.[19] In this nanocavity, the plasmon excitation induced by inelastic

electron tunneling is largely suppressed due to increased distance between two metal leads. We thus consider only the direct excitation of the molecule by the tunneling currents and have ignored the molecular excitation due to the plasmon pumping. To obtain the luminescence spectra, we evaluate two essential quantities of the molecule: the radiative decay rate and the state population at the dynamic equilibrium.
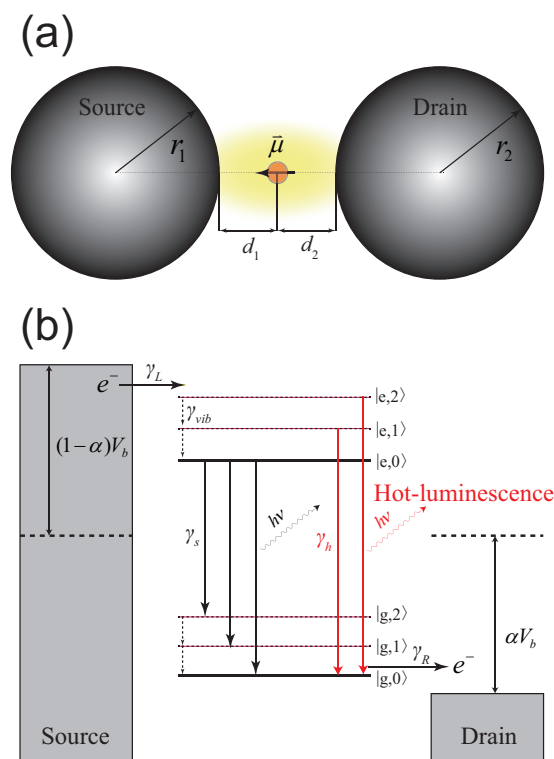
Fig. 1 (a) Schematic picture of the system setup. The tunneling junction is modeled with two metal spheres and the molecule is treated as an electric dipole locating on the axis of the dimer (we set $r_1 = r_2 = r$, $d_1 = d_2 = d/2$ hereafter). (b) Schematic diagram of energy levels and various transition processes within the system formed by a molecule in a tunnel junction. $|g, v\rangle$ and $|e, v\rangle$ stands for the ground and excited electronic states respectively, with v denoting the vibrational quantum number. γ_L (γ_R) is the bare tunneling rate of electrons between the molecule and the left (right) lead; γ_{vib}, γ_s and γ_h are the vibrational damping, spontaneous emission and hot-luminescence rate, respectively. In our simulations, we set $\gamma_L = \gamma_R = 10^{10}$ s^{-1} and $\gamma_{vib} = 10^{12}$ s^{-1}, based on physically realistic tunneling currents (~ 100 pA) and picosecond vibrational lifetime for porphyrin molecules. The coupling coefficient is chosen to be $\alpha = 1/2$.[21]

Our theoretical modeling is based on a microscopic multiscale treatment that combines the classical electrodynamics with quantum mechanics. The spontaneous decay rate is obtained by generalized Mie theory.[24] Using d-parameter methods,[25–27] we have also taken into account non-local correc-

tions, which becomes dominant when the molecule is closely located above the metal. The molecule is modeled as an electric dipole inside the tunnel junction, which is approximated by two identical spheres shown in Fig. 1(a). The direction of the dipole is set parallel to the axis of the dimer in all the calculations unless otherwise specified. The material of the dimer is chosen to be silver or gold, which is commonly used in the STML experiments.

Within the framework of quantum master equation, the various dynamic processes are considered to obtain the state population of the molecule at the dynamic equilibrium. As illustrated in Fig. 1(b), the molecule is simulated as a two-level system with only one vibrational mode for simplicity. The equation of motion of the density matrix ρ for the model molecule is[21,25,28]

$$\frac{d\rho}{dt} = \frac{1}{i\hbar}[H_0, \rho] + (\mathscr{L}_{\text{tun}} + \mathscr{L}_{\text{damp}} + \mathscr{L}_{\text{deph}})\rho, \qquad (1)$$

where H_0 is the free molecular Hamiltonian. The three Liouvillian operators describing different dynamic processes are detailed below.

The Liouvillian operator $\mathscr{L}_{\text{tun}}$ accounts for the electron tunneling between the molecule and the left or right lead of the tunneling junction. Assuming this transition would only modify the population of the molecule, i.e., the diagonal elements of the density matrix ρ, we thus have the rate-equation form[20–22]

$$\mathscr{L}_{\text{tun}}\rho = -\sum_{ij}(\gamma_{\text{tun}}^{j\to j}\sigma_{ii}\rho\sigma_{ii} - \gamma_{\text{tun}}^{j\to i}\sigma_{ij}\rho\sigma_{ji}), \qquad (2)$$

where $\gamma_{\text{tun}}^{j\to j}$ is the tunneling induced transition rate from the ith level of molecule to the jth level considering the Fermi distribution function of the leads and Franck-Condon factors,[22] σ_{ij} is a square matrix of dimension $2 \times N_{\text{vib}}$ with element (i, j) equals 1 while all other elements vanish; N_{vib} is the number of the vibrational levels for each electronic state.

The Liouvillian operator $\mathscr{L}_{\text{damp}}$ describing damping processes is decomposed into three parts: $\mathscr{L}_{\text{damp}} = \mathscr{L}_{\text{Rad}} + \mathscr{L}_{\text{NR}} + \mathscr{L}_{\text{vib}}$, which accounts for radiative decay, non-radiative decay and vibrational relaxation, respectively. The damping of the electronic state has the Lindblad form[25,28]

$$\mathscr{L}_{\text{Rad,NR}}\rho = -\sum_{i\in g, j\in e}\frac{\gamma_{\text{Rad,NR}}^{j\to i}}{2}(\sigma_{ji}\sigma_{ij}\rho - 2\sigma_{ij}\rho\sigma_{ji} + \rho\sigma_{ji}\sigma_{ij}), \qquad (3)$$

where $\gamma_{\text{Rad,NR}}^{j\to i}$ is the transition rate from jth to ith level for the radiative or non-radiative process. These transition rates are obtained by the generalized Mie theory with non-local corrections[24,25] and further modified by the Franck-Condon factors.[21] The term $\mathscr{L}_{\text{vib}}$ characterizing vibrational relaxations

can be written as[20]

$$\mathscr{L}_{\text{vib}}\rho = -\gamma_{\text{vib}}\sum_i\left(\sigma_{ii}\rho\sigma_{ii} - \frac{e^{-\frac{\hbar\omega_{\text{vib}}^i}{k_BT}}\sum_j\sigma_{ij}\rho\sigma_{ji}}{\sum_k e^{-\frac{\hbar\omega_{\text{vib}}^k}{k_BT}}}\right), \qquad (4)$$

where γ_{vib} is the vibrational relaxation rate, and the energy levels i, j and k should belong to the same electronic state because the vibrational damping is an intraband transition. We note that $\gamma_{\text{Rad}}^{j\to i}$ and $\gamma_{\text{NR}}^{j\to i}$ describe the modified decay rates of the molecule in the nanocavity. Essentially, it is the variation of these rates that are responsible for the spectral modulation and HL.

The last Liouvillian term $\mathscr{L}_{\text{deph}}$ describes the dephasing of interband coherence[25]

$$\mathscr{L}_{\text{deph}} = -\gamma_{\text{deph}}\sum_{i\in g, j\in e}(\sigma_{ij}\rho_{ij} + \sigma_{ji}\rho_{ji}), \qquad (5)$$

where γ_{deph} is the dephasing rate.

By solving Eq. (1) with the Liouvillian terms described above, we can obtain the steady state population of the molecule at dynamic equilibrium, then the spontaneous emission spectra can be simply described by Lorentzian function as[21]

$$I(\omega) \propto \frac{\Gamma}{2\pi}\sum_{i\in g, j\in e}\frac{\gamma_{\text{Rad}}^{j\to i}\rho_{jj}^s}{(\omega - \omega_{ji})^2 + (\Gamma/2)^2}, \qquad (6)$$

where Γ is the full width at half maximum of the molecular emission spectra, and ρ_{jj}^s is the steady state population.

3 Effects of plasmonic nanocavity on spontaneous decay rates

In vacuum, the spontaneous emission of a molecule is a pure quantum phenomenon, which originates from the interaction between the transition dipole and the vacuum fluctuations of the quantized electromagnetic fields. The presence of dielectric materials surrounding the molecule will modify the photon density of states, and therefore change the spontaneous decay rate, known as the Purcell effect.[29,30] A metallic plasmonic nanocavity is known to act as an efficient optical antenna[31] and can increase the local density of optical states dramatically. Such effect corresponds to the increase of the strength of vacuum fluctuations of plasmons (i.e., plasmonic vacuum field), which can lead to dramatic enhancement of the molecular spontaneous decay rates. However, because of the large dissipation of the metal, the near-field photons generated from the spontaneous decay of the molecule near metals
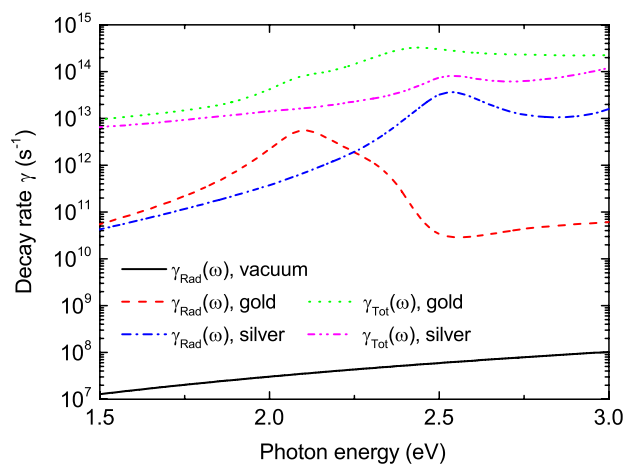
Fig. 2 Radiative $\gamma_{\text{Rad}}(\omega)$ and total $\gamma_{\text{Tot}}(\omega)$ decay rates for an electric dipole ($\mu_z = 1$ eÅ) placed in vacuum, or within a gold dimer and silver dimer ($d = 1$ nm, $r = 30$ nm), respectively.

may not be able to propagate to the far field (i.e., the non-radiative decay). In this section, we discuss briefly the relation between the spontaneous decay rate and the plasmonic nanocavity structures, and also the relation between the radiative and non-radiative decay rates.

For an ideal point electric-dipole μ in vacuum, the spontaneous decay rate contains only the radiative component and can be evaluated as $\gamma_{\text{Rad}}^0(\omega) = \frac{\omega^3 \mu^2}{3\pi\hbar\varepsilon_0 c^3}$. As depicted in Fig. 2, when placed in the nanocavity, the radiative decay rate $\gamma_{\text{Rad}}(\omega)$ of the molecule is increased by 3 to 5 orders of magnitude in optical wavelengths,[32–35] driving the radiative lifetime into the picosecond (ps) or even sub-ps regime.[36,37] By comparing the radiative $\gamma_{\text{Rad}}(\omega)$ and total $\gamma_{\text{Tot}}(\omega)$ decay rates, we also see the presence of a large portion of non-radiative decay. To facilitate the comparison between different decay rates, we define the radiative enhancement factor $M_{\text{Rad}}(\omega) = \gamma_{\text{Rad}}(\omega)/\gamma_{\text{Rad}}^0(\omega)$ and the quantum efficiency $\eta(\omega) = \gamma_{\text{Rad}}(\omega)/\gamma_{\text{Tot}}(\omega)$. Clearly, to achieve efficient spontaneous emission of molecules in a plasmonic nanocavity, we need both M_{Rad} and η to be large.

Figure 3 displays the profiles of $M_{\text{Rad}}(\omega)$ and $\eta(\omega)$ for the nanocavities with different geometries and materials. As shown in Figs. 3(a) and (b), for the silver dimers with a fixed gap size d, the peak value of M_{Rad} increases dramatically with decreasing radii, while η shows a peak maximum around $r = 30$ nm (but not so substantially different for other sizes). Note that the enhancement behavior could be different not only for different sizes, but also for different materials. For the gold dimers, when the radius decreases from 60 to 20 nm, the peak value of both M_{Rad} and η first increases and then decreases, as shown in Fig. 3(e) and (f). The dramatical decrease of the value for large frequency is due to the interband transi-

tion loss in gold above ~ 2 eV.[38] Nevertheless, one thing is common: the plasmonic resonance frequency shows considerable blueshift with decreasing radii for both gold and silver dimers.[39]

Another important control parameter in the dimer nanocavities is the gap size d between the two spherical particles.[24] In Fig. 3(c) we show the profile of M_{Rad} for a silver dimer with a fixed radius $r = 30$ nm. As the gap size d decreases, the resonance peak shifts towards red gradually within a few tenth of eV, but the peak value strongly increases, indicating a very large increase in the local density of optical states (or photonic mode density) at the gap region. However, the molecule in a smaller gap is much closer to the metal surface, and therefore in conjunction with an enhanced radiative decay, it also suffers from a larger non-radiative decay.[37,40,41] It can be seen from Figs. 3(d) and (h) that the quantum efficiencies decrease more rapidly at very small distances, suggesting an ever-important role of non-radiative decay in these situations. The gold dimer shows a similar trend for the peak value of M_{Rad} and η, except for a weakened enhancement at relatively higher energy due to the interband transition. Generally speaking, gold has relatively smaller enhancement factors and quantum efficiency than silver due to its larger imaginary component of the dielectric constant and resultant larger optical loss.[38]

4 Effects of plasmonic nanocavity on molecular hot luminescence

The vibrational damping rate of the molecule is typically 10^{12} s^{-1}, which is much larger than the vacuum spontaneous emission rate of free-space molecules around 10^8 s^{-1}. Therefore, the excited molecule in free space follows the Kasha's rule and will relax to the vibrational ground state $|e, \nu = 0\rangle$ before making a radiative transition from the electronic excited state to the ground state. However, this radiating-after-cooling dynamics of the molecule can be drastically changed in a plasmonic nanocavity, as the spontaneous decay rate is dramatically enhanced, enabling the radiative process to become competitive to the vibrational relaxation.

As shown in the previous section, the spontaneous decay of the molecule can be enhanced by several orders of magnitude. Such dramatic enhancement suggests that once excited, the molecule may go through the radiative decay before cooling down to $|e, 0\rangle$, as shown below. By inserting the corresponding decay rates into the quantum master equation [i.e., Eq. (1)], we obtain the emission spectra of the molecule in Fig. 4. In the following, we discuss the effect of two key parameters on the molecular emission spectra, namely the dipole moment $\vec{\mu}$ and the quantum efficiency η, the latter reflects the branching ratio of radiative versus non-radiative decay, which depends
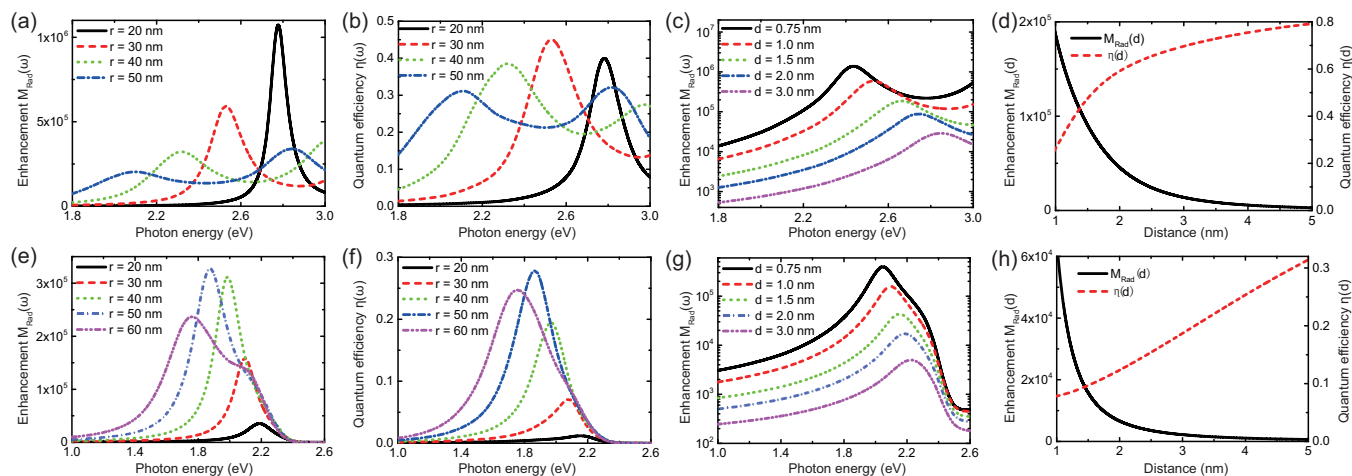
Fig. 3 Radiative enhancement factor M_{Rad} and quantum efficiency η in the tunnel junction for silver dimers [(a)-(d)] and gold dimers [(e)-(h)] with a dipole moment $\mu = 1$ eÅ. In (a), (b), (e) and (f), $d = 1$ nm; in (c) and (g), $r = 30$ nm; in (d) and (h), the calculations are done at $r = 40$ nm with an energy of 2.5 and 1.8 eV, respectively.
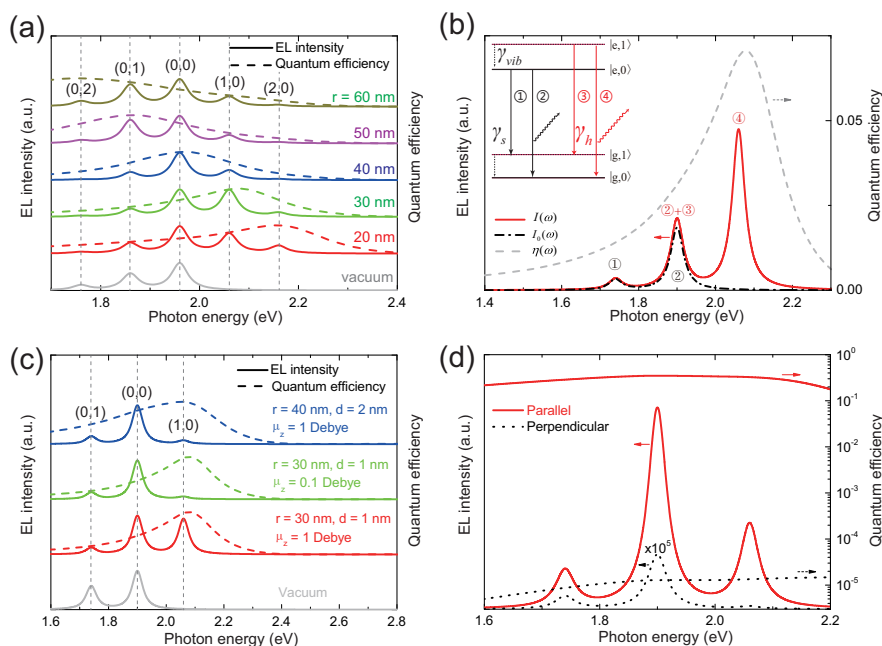
Fig. 4 (a) Molecular fluorescence spectra in vacuum and in a tunnel junction for gold dimers ($r = 20 - 60$ nm, $d = 1$ nm), with the molecular optical band gap $\varepsilon_0 = 1.96$ eV, vibrational energy $\hbar\omega_{vib} = 0.10$ eV, $N_{vib} = 3$ and $\mu_z = 1$ Debye. (b) Illustration of contributions from different channels for molecular emission ($\varepsilon_0 = 1.90$ eV, $\hbar\omega_{vib} = 0.16$ eV, $\mu_z = 1$ eÅ) in the junction of a gold dimer ($r = 30$ nm, $d = 1$ nm). (c) Molecular fluorescence spectra in the junction of a gold dimer, with $\varepsilon_0 = 1.90$ eV, $\hbar\omega_{vib} = 0.16$ eV and $N_{vib} = 2$. (d) Molecular fluorescence spectra and quantum efficiency for electric dipoles ($\mu = 1$ eÅ) parallel and perpendicular to the axis of the gold dimer ($r = 40$ nm, $d = 2$ nm). Note that the emission spectra for the latter has been multiplied by a factor of 10^5. Non-local corrections were not considered in the calculation of (d). Parameters physically realistic for the STML experiments [19] were adopted in these simulations for the particle diameter, gap distance, molecular optical band gap, vibrational energy and dipole size.

on resonant conditions.

In vacuum, the relative intensities of the different emission channels are determined mainly by the Franck-Condon factors. Nevertheless, in the plasmonic nanocavity, for the normal emission channels decaying from $|e,0\rangle$ that follows the Kasha's rule, the relative intensities of spectral peaks can be further modified by the plasmon resonance conditions associated with the nanocavity configuration. As shown in Fig. 4(a), the emission spectra of the molecule in the nanocavity could deviate profoundly from that of the molecule in vacuum.[19] Evidently, we can see that the relative intensities of these normal emission peaks are correlated with the quantum efficiencies $\eta(\omega)$, which are energy dependent, with the peak maximum corresponding to the plasmon resonance for different nancavity configurations (Fig. 3). More remarkably, when the nanocavity plasmon is tuned to resonate with the molecular vibronic transition from higher vibrational excited states [e.g., (1,0) and (2,0) in Fig. 4(a)], some new peaks also appear at higher energies and can be identified as the HL emission. This is because their energies are higher than the zero-phonon line (0,0) of the molecule and can only be obtained from the direct radiative decay of the excited vibrational states $|e, v > 0\rangle$. In other words, tuning the plasmonic resonance modes by geometry and material (Fig. 3) will allow us to not only shape the spectral profile of molecular emissions, but also to generate the HL without vibrational relaxation, as demonstrated theoretically here in Fig. 4(a) and also experimentally in Ref. 19.

It is worthy to point out that all the resonant enhancement observed in the spectral shaping and HL can be reasonably explained in terms of the emission rates enhancement alone, without the need to assume additional plasmonic pumping in the molecular excitation process. Actually, the inclusion of very weak plasmonic excitation by inelastic tunneling electrons in the model would only add a very weak and broad emission background to the sharp molecule-specific emission peaks, essentially the same as what is presented in Fig. 4. On the other hand, if the plasmons can be effectively excited by tunneling electrons, the photons generated would be dominated by plasmonic emission, featuring a very broad emission band with weak (or even negligible) decorations of dips or peaks associated with molecules,[42–46] which is against the spectral feature observed experimentally in Ref. 19. We would also like to emphasize the dominant competing factor for the HL generation physically observed: it is probably not the large electron transmission rate but rather the large spontaneous emission rate (namely, a large Purcell effect) that is responsible for the occurrence of HL. The central message delivered here is: both spectral shaping and the occurrence of hot electroluminescence experimentally observed in the STM induced molecular emission are mainly due to the enhancement of the spontaneous emission rate in plasmonic vacuum field

rather than the presence of plasmon stimulated emission. Such enhancement mechanism is believed to be very important for the electron-induced electroluminescence process, though the situation could be quite different for photon-induced photoluminescence, where the pumping of molecules by plasmons induced by incident lasers could play a critical role in many cases, particularly when strong plasmonic fields are resonantly excited.[47–49]

Apart from the new peaks, the change of the relative intensity in normal luminescence may also imply the occurrence of the HL process. In order to see this more clearly, we consider a further simplified system containing only one vibrational excited level shown in the inset of Fig. 4(b), where $I(\omega)$ is the full emission spectra while $I_0(\omega)$ only accounts for ① and ② which are the only two possible decay channels in vacuum. In the nanocavity, two new luminescence channels ③ and ④ are turned on by the enhanced spontaneous decay rate. The channel ④ will provide a new emission peak, which can be easily identified as the HL. However, the "hot" nature of the channel ③ is barely noticed before. This channel has the same transition energy as channel ② and therefore will also change the relative intensity of this emission peak.

The occurrence of HL and its amplitude depends strongly on the competition between the radiative decay rate γ_{Rad} and the vibrational damping rate γ_{vib}. As shown in Fig. 4(c), even assuming a similar quantum efficiency profile for the emitter, the HL feature is closely related to the size of the dipole moment and the gap distance. The increase in either parameter alone is not sufficient to generate considerable HL (top two solid spectra). This is because, according to the Fermi's golden rule, the emission rate is related to both the dipole moment and the local density of optical states. The HL feature starts to show up distinctly only when the molecule has a sizable dipole moment and simultaneously, the photon mode density at the emitter (or the enhancement factor) is sufficiently large through decreasing the gap distance, both favoring a large emission rate for the HL channel.

A comparatively large transition dipole component parallel to the axis of the dimer also appears crucial for the generation of molecular fluorescence as well as HL. It is well known that the fluorescence from a dipole parallel to the substrate is often quenched. As depicted in Fig. 4(d), for a dipole oriented perpendicular to the axis of the dimer, the emission of the molecule is dramatically quenched due to the much smaller quantum efficiency ($\sim 10^{-5}$) caused by a much smaller radiative decay rate. In a word, high quantum efficiencies are sufficient to produce normal luminescence, but to generate HL, both quantum efficiency and radiative enhancement factor need to be relatively large.

5 Conclusions

In summary, we have investigated the effect of the molecular HL induced by tunneling currents from a plasmonic nanocavity formed by the junction of two metal nanospheres using physically realistic parameters. According to our electromagnetic simulations based on generalized Mie theory with non-local corrections, we have shown that in the nanocavity, both the spontaneous decay rate and quantum efficiency of the molecule can be dramatically modulated by carefully tuning the geometry and material of the nanocavity. Furthermore, within the framework of quantum master equation, our calculations for a model system containing both electronic and vibrational decay processes indicate that, in contrast to Kasha's rule, the excited molecule in a resonant plasmonic nanocavity can directly decay radiatively to the ground state without invoking vibrational relaxation. This is made possible because the radiative decay rate is enhanced by several orders of magnitude for a plasmonic nanocavity with gap distances around 1 nm, which enables the radiative process to occur on the lifetime scale of picoseconds or even sub-picoseconds[37] and, as a result, to become competitive to the vibrational relaxation. The role of a resonant plasmonic nanocavity can also be viewed as to enhancing the field strength of vacuum fluctuations at the emitter, thus leading to increased local density of optical states and resultant enhanced spontaneous emission rates according to the Fermi's golden rule. Such enhancement in the plasmonic vacuum field alone is sufficient to explain the spectral shaping and HL observed experimentally, without invoking plasmon stimulated emission. In other words, when the STM tip is positioned on top of a molecule, the plasmon-exciton coupling can be usually classified into the weak coupling regime, i.e., essentially a unidirectional energy transfer from molecular excitons to nanocavity plasmons. Such understanding of emission enhancement in terms of increased radiative decay rates by resonant plasmons is believed to be important not only for single-molecule EL but also for single-molecule Raman scattering,[19,50] and may be instructive for the development of molecular plasmonics and optoelectronics.

Acknowledgements

References

1 J. K. Gimzewski, B. Reihl, J. H. Coombs and R. R. Schlittler, *Z. Phys. B*, 1988, **72**, 497–501.
2 R. Berndt, J. K. Gimzewski and P. Johansson, *Phys. Rev. Lett.*, 1991, **67**, 3796–3799.
3 Y. Uehara, T. Fujita and S. Ushioda, *Phys. Rev. Lett.*, 1999, **83**, 2445–2448.
4 N. Nilius, N. Ernst and H.-J. Freund, *Phys. Rev. Lett.*, 2000, **84**, 3994–3997.
5 G. Hoffmann, J. Kliewer and R. Berndt, *Phys. Rev. Lett.*, 2001, **87**, 176803.
6 D. Hone, B. Mühlschlegel and D. J. Scalapino, *Appl. Phys. Lett.*, 1978, **33**, 203–204.
7 R. W. Rendell, D. J. Scalapino and B. Mühlschlegel, *Phys. Rev. Lett.*, 1978, **41**, 1746–1750.
8 P. Johansson, R. Monreal and P. Apell, *Phys. Rev. B*, 1990, **42**, 9210–9213.
9 B. N. J. Persson and A. Baratoff, *Phys. Rev. Lett.*, 1992, **68**, 3224–3227.
10 J. Aizpurua, S. P. Apell and R. Berndt, *Phys. Rev. B*, 2000, **62**, 2065–2073.
11 R. Berndt, R. Gaisch, J. K. Gimzewski, B. Reihl, R. R. Schlittler, W. D. Schneider and M. Tschudy, *Science*, 1993, **262**, 1425–1427.
12 X. H. Qiu, G. V. Nazin and W. Ho, *Science*, 2003, **299**, 542–546.
13 Z. C. Dong, X. L. Guo, A. S. Trifonov, P. S. Dorozhkin, K. Miki, K. Kimura, S. Yokoyama and S. Mashiko, *Phys. Rev. Lett.*, 2004, **92**, 086801.
14 E. Ćavar, M.-C. Blüm, M. Pivetta, F. Patthey, M. Chergui and W.-D. Schneider, *Phys. Rev. Lett.*, 2005, **95**, 196102.
15 C. Chen, P. Chu, C. A. Bobisch, D. L. Mills and W. Ho, *Phys. Rev. Lett.*, 2010, **105**, 217402.
16 F. Rossel, M. Pivetta and W.-D. Schneider, *Surf. Sci. Rep.*, 2010, **65**, 129–144.
17 H. Liu, Y. Ie, T. Yoshinobu, Y. Aso, H. Iwasaki and R. Nishitani, *Appl. Phys. Lett.*, 2006, **88**, 061901.
18 F. Rossel, M. Pivetta, F. Patthey and W.-D. Schneider, *Opt. Express*, 2009, **17**, 2714–2721.
19 Z. C. Dong, X. L. Zhang, H. Y. Gao, Y. Luo, C. Zhang, L. G. Chen, R. Zhang, X. Tao, Y. Zhang, J. L. Yang and J. G. Hou, *Nat. Photon.*, 2010, **4**, 50–54.
20 J. S. Seldenthuis, H. S. J. van der Zant, M. A. Ratner and J. M. Thijssen, *Phys. Rev. B*, 2010, **81**, 205430.
21 G. Tian, J. C. Liu and Y. Luo, *Phys. Rev. Lett.*, 2011, **106**, 177401.
22 G. Tian and Y. Luo, *Phys. Rev. B*, 2011, **84**, 205419.
23 Y. Zhang, Y. Zelinskyy and V. May, *Phys. Rev. B*, 2013, **88**, 155426.

24 M. Ringler, A. Schwemer, M. Wunderlich, A. Nichtl, K. Kürzinger, T. A. Klar and J. Feldmann, *Phys. Rev. Lett.*, 2008, **100**, 203002.

25 P. Johansson, H. Xu and M. Käll, *Phys. Rev. B*, 2005, **72**, 035427.

26 A. Liebsch, *Phys. Rev. B*, 1987, **36**, 7378–7388.

27 B. N. J. Persson and A. Baratoff, *Phys. Rev. B*, 1988, **38**, 9616–9627.

28 M. O. Scully and M. S. Zubairy, *Quantum Optics*, Cambridge University Press, 1997.

29 E. M. Purcell, *Phys. Rev.*, 1946, **69**, 681.

30 A. N. Oraevskii, *Phys.-Usp.*, 1994, **37**, 393–405.

31 J.-W. Liaw, J.-H. Chen, C.-S. Chen and M.-K. Kuo, *Opt. Express*, 2009, **17**, 13532–13540.

32 C.-H. Cho, C. O. Aspetti, M. E. Turk, J. M. Kikkawa, S.-W. Nam and R. Agarwal, *Nat. Mater.*, 2011, **10**, 669–675.

33 A. Kinkhabwala, Z. Yu, S. Fan, Y. Avlasevich, K. Müllen and W. E. Moerner, *Nat. Photon.*, 2009, **3**, 654–657.

34 K. J. Russell, T.-L. Liu, S. Cui and E. L. Hu, *Nat. Photon.*, 2012, **6**, 459–462.

35 G. M. Akselrod, C. Argyropoulos, T. B. Hoang, C. Ciracì, C. Fang, J. Huang, D. R. Smith, and M. H. Mikkelsen, *Nat. Photon.*, 2014, **8**, 835–840.

36 C. M. Galloway, P. G. Etchegoin and E. C. LeRu, *Phys. Rev. Lett.*, 2009, **103**, 063003.

37 X.-W. Chen, M. Agio and V. Sandoghdar, *Phys. Rev. Lett.*, 2012, **108**, 233001.

38 P. B. Johnson and R. W. Christy, *Phys. Rev. B*, 1972, **6**, 4370–4379.

39 S. Foteinopoulou, J. P. Vigneron and C. Vandenbem, *Opt. Express*, 2007, **15**, 4253–4267.

40 P. Anger, P. Bharadwaj and L. Novotny, *Phys. Rev. Lett.*, 2006, **96**, 113002.

41 G. Baffou, C. Girard, E. Dujardin, G. C. des Francs and O. J. F. Martin, *Phys. Rev. B*, 2008, **77**, 121101(R).

42 A. Lovera, B. Gallinet, P. Nordlander and O. J. F. Martin, *ACS Nano*, 2013, **5**, 4527–4536.

43 N. L. Schneider and R. Berndt, *Phys. Rev. B*, 2012, **86**, 035445.

44 S. Mühlenberend, N. L. Schneider, M. Gruyters and R. Berndt, *Appl. Phys. Lett.*, 2012, **101**, 203107.

45 Y. Zhang, F. Geng, H. Y. Gao, Y. Liao, Z. C. Dong and J. G. Hou, *Appl. Phys. Lett.*, 2010, **97**, 243101.

46 T. Lutz, C. Große, C. Dette, A. Kabakchiev, F. Schramm, M. Ruben, R. Gutzler, K. Kuhnke, U. Schlickum and K. Kern, *Nano Lett.*, 2013, **13**, 2846–2850.

47 H. Yuan, S. Khatua, P. Zijlstra, M. Yorulmaz and M. Orrit, *Angew. Chem. Int. Ed.*, 2013, **52**, 1217–1221.

48 Y.-L. Wang, F. Nan, X.-L. Liu, L. Zhou, X.-N. Peng, Z.-K. Zhou, Y. Yu, Z.-H. Hao, Y. Wu, W. Zhang, Q.-Q. Wang and Z. Zhang, *Sci. Rep.*, 2013, **3**, 1861.

49 G. Lu, J. Liu, T. Zhang, H. Shen, P. Perriat, M. Martini, O. Tillement, Y. Gu, Y. He, Y. Wanga and Q. Gong, *Nanoscale*, 2013, **5**, 6545–6551.

50 R. Zhang, Y. Zhang, Z. C. Dong, S. Jiang, C. Zhang, L. G. Chen, L. Zhang, Y. Liao, J. Aizpurua, Y. Luo, J. L. Yang and J. G. Hou, *Nature*, 2013, **498**, 82–86.